Available online at www.sciencedirect.com
ScienceDirect
Trans. Nonferrous Met. Soc. China 19(2009) 19−25
Transactions of Nonferrous Metals Society of China
www.tnmsc.cn

Effect of melt superheat on microstructure of Al4Fe2Mn1.5 Monel alloy

WANG Fu(王 富), ZOU Jun-tao(邹军涛), WANG Xian-hui(王献辉), FAN Zhi-kang(范志康)

Shaanxi Key Laboratory for Electrical Materials and Infiltration Technology,
Xi'an University of Technology, Xi'an 710048, China

Received 7 January 2008; accepted 31 March 2008

Abstract: The effect of melt superheat on microstructure of Al4Fe2Mn1.5 Monel alloy made by vacuum melting method was studied. The results show that the alloy consists of dendritic γ matrix and γ' phase, wherein γ' phase has two morphologies at different melt superheat. One is divorced eutectic γ' which distributes in the interdendritic area, the other distributes dispersedly in single particle on the dendritic arm and exists in the petalform shape in the transition area between dendritic arm and interdendritic area. With the increase of superheat, the dendrite becomes finer, the primary dendritic arm is melted off and the secondary dendritic arm spacing decreases. The size of γ' phase distributed on the dendritic arm becomes smaller and the divorced eutectic γ' phase increases.

Key words: Al4Fe2Mn1.5 Monel alloy; melt superheat; microstructure

1 Introduction

Monel alloy is a nickel based Ni-Cu alloy with 70% Ni and 30% Cu (mass fraction)[1]. Al addition into Ni-Cu alloy can improve its strength and corrosion resistance[2]. The Monel alloy containing Al is widely used as structural parts[3−5] in the circumstances of sea water, acid, alkali and salt due to its excellent corrosion resistance and high strength. For example, it is often used as pumping rods and oil-well instruments in the petroleum and gas industry and the important components of pipeline used in ship in the shipbuilding industry[6−7]. Besides, it is also used as the scalpel in surgical operations and electron components in electronic industry[8].

Recently, most investigations of Monel alloy with Al addition are focused on the heat treatment[6, 9−13]. Few are studied on the effect of melting process on microstructure of this alloy. Both the size of dendrite and the percentage of precipitated γ' phase intensively depend on melting process and solidification process. In fact, the melting temperature represents melt superheat, which has a great effect on liquid structure, as-cast microstructure and combination of properties of the alloy. In the present investigation, the effect of melt superheat on the microstructure of Al4Fe2Mn1.5 alloy is studied and the goal is to improve as-cast microstructure and properties of the alloy by adjusting the melt superheat.

2 Experimental

The composition of Al4Fe2Mn1.5 Monel alloy is listed in Table 1. The NiCu60Mn3Fe4Al8 was used as the master alloy in the experiment. The four kinds of alloys were prepared in the ZRS−18Q computer controlled vacuum sintering furnace. After the raw material was melted, it was held for 60 min with different superheating of 50, 100, 150 and 200 ℃, and then cooled in the furnace. The samples were cut from the four cast ingots on the same location. The etching agent was 20 g $CuSO_4$ + 100 mL HCl + 5 mL H_2SO_4 + 80 mL H_2O. The microstructure was analyzed by OLYMPUS vertical optical microscope, JEM−3010 transmission electron microscope, XRD−7000S X-ray diffraction instrument, JSM−6700F scanning electron microscope and Oxford INCA energy spectrometer.

Table 1 Nominal chemical composition of Al4Fe2Mn1.5 Monel alloy (mass fraction, %)

Cu	Mn	Fe	Al	Ni
30	1.5	2	4	Bal.

Corresponding author: FAN Zhi-kang; Tel: +86-29-82312773; E-mail: fanzk@xaut.edu.cn
DOI: 10.1016/S1003-6326(08)60222-8

3 Results

3.1 Microstructure of Al4Fe2Mn1.5 Monel alloy

The test samples made with different superheat were studied by OM, SEM, EDS, XRD and TEM. The results show that Al4Fe2Mn1.5 Monel alloy consists of γ matrix and γ' phase. Fig.1 shows XRD pattern of Al4Fe2Mn1.5 Monel alloy with melt superheat of 200 ℃.

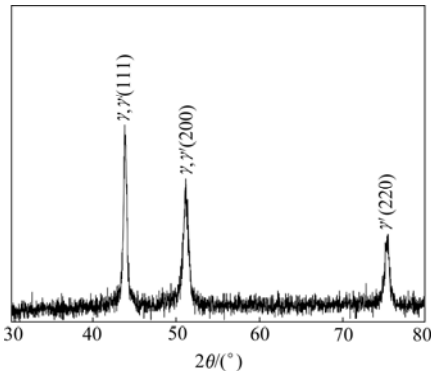

Fig.1 XRD pattern of Al4Fe2Mn1.5 Monel alloy with melt superheat of 200 ℃

The γ matrix is Ni-Cu solid solution which contains some fractions of Mn, Fe and Al elements (as listed in Table 2). In the as-cast state, the morphology of γ matrix exists in dendrite, as seen in Fig.2.

From the diffraction pattern (as shown in Fig.3 and Fig.4), the calculated results show that γ' phase is Ni_3Al intermetallic compound, which has two morphologies. One distributes dispersedly as single particle on dendritic arms and in petalform shape in the transition areas between dendritic arms and interdendritic areas (as indicated in zone B and C in Fig.5 and Fig.3). From the diffraction pattern shown in Fig.3, γ' phase has superlattice structure. It is the diffraction pattern of [001] zone axis and the diffraction pattern is stack of γ' phase and γ solid solution. In addition, the relationship between γ' phase and γ matrix is in absolute coherence. The other is divorced plateform eutectic γ' which distributes in the interdendritic areas (as shown in zone A in Fig.5 and Fig.4). Fig.4 shows the diffraction pattern of [012] zone axis of γ' phase. Besides, the molar ratio of Ni to Al is approximately 3 (as listed in Table 3). It is further verified that the phase is confirmed to be γ' phase. The phase exists in the plateform and there is no coexistence between two phases. It is indicated that during the solidification, as there is more primary γ phase and fewer liquid, the γ phase in the eutectic is combined with primary γ phase and pushes γ' phase to the interdendritic area, thus forming divorced eutectic completely.

Table 2 EDS results of dendritic γ matrix

Element	Mass fraction/%	Mole fraction/%
Cu	22.84	20.65
Mn	0.42	0.44
Fe	2.51	2.58
Al	3.22	6.85
Ni	71.01	69.48

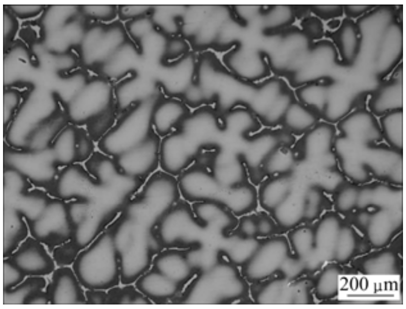

Fig.2 Microstructure of γ phase

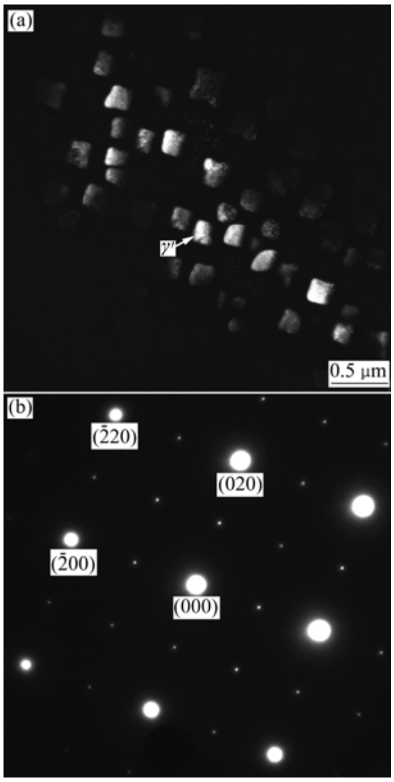

Fig.3 TEM image and diffraction pattern of zone axis [001] of γ' on dendritic arm and in transition area between dendritic arm and interdendritic area

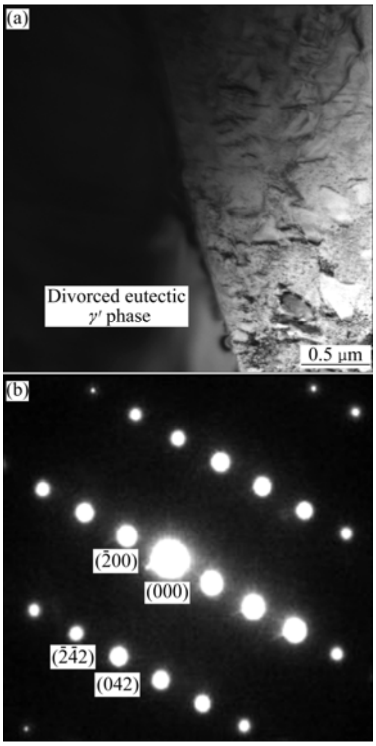

Fig.4 TEM image and diffraction pattern of zone axis [012] of divorced eutectic γ′ in interdendritic area

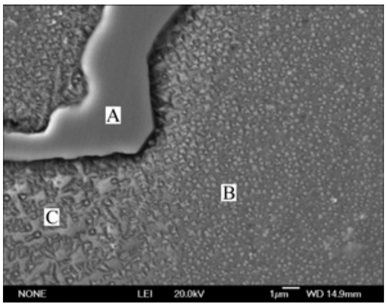

Fig.5 SEM micrograph of Al4Fe2Mn1.5 Monel alloy with melt superheat of 200 ℃

Table 3 EDS results of devoiced eutectic γ′ in interdendritic area

Element	Mass fraction/%	Mole fraction/%
Al	15.61	28.69
Ni	84.39	71.31

3.2 Effect of melt superheat on microstructure of Al4Fe2Mn1.5 Monel alloy

Fig.6 shows the dendritic morphologies of γ matrix at different melt superheat. When the melt superheat is 50 ℃, the dendrite is coarse. As the melt superheat increases, it becomes finer and the primary dendrite arms are melted off gradually. The secondary dendrite arm spacing(SDAS) at different melt superheat is shown in

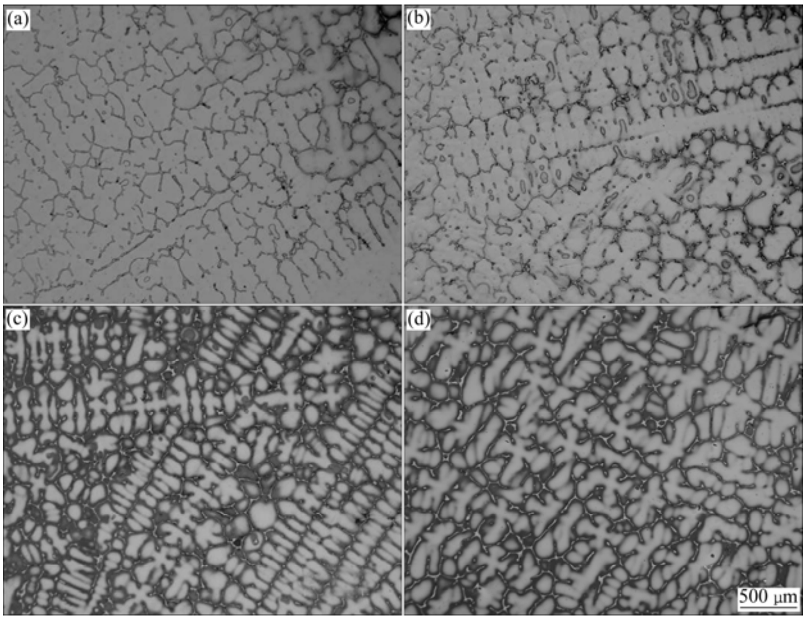

Fig.6 Dendritic morphologies of Al4Fe2Mn1.5 Monel alloy at different melt superheat: (a) 50 ℃; (b) 100 ℃; (c) 150 ℃; (d) 200 ℃

Fig.7. It can be seen that the SDAS becomes finer with increasing melt superheat.

Fig.8 shows the morphologies of eutectic γ′ phase at different melt superheat. The area ratios of eutectic γ′ phase at corresponding melt superheat that were calculated by Digital Micrograph software are shown in Fig.9. From these two figures, it can be got that with the increase of melt superheat, the fraction of divorced eutectic γ′ phase increases.

Fig.10 and Fig.11 show the morphologies and average diameters of γ′ phase at different melt superheat, respectively. It can be seen that the average diameter of γ′ phase gradually becomes finer with the increase of melt superheat.

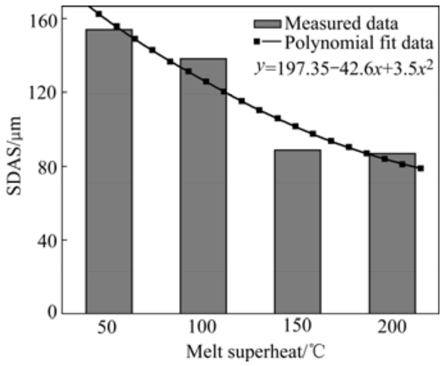

Fig.7 Secondary dendrite arm spacing of Al4Fe2Mn1.5 Monel alloy at different melt superheat

4 Discussion

Diffusion coefficient is one of the important physical properties in liquid metal and alloy, which has an obvious effect on the distribution of elements, crystal growth rate and segregation in solidification process. The factors influencing the diffusion coefficient are temperature and composition. In the present investigation, the main factor is temperature[14] due to a constant composition. The relationship between diffusion coefficient and temperature can be expressed as exponential law by many theoretical studies and experiments:

$$D^* = D_0^* \exp\left(\frac{-E_\mathrm{D}}{RT}\right) \qquad D^* = D_0^* \exp\left(\frac{-E_D}{RT}\right)$$

(1) ~~(4-1)~~

~~W~~where D^* ~~Self~~ is the self-diffusion coefficient; D_0^* is the ~~c~~ ~~C~~constant; E_D is the ~~D~~diffusion activation energy.

From the formula, it can be deduced that the self-diffusion coefficient increases with increasing melt superheat. In the experiments, Al atom exists as a big irreversible Ni_3Al-like intermediate ordered atom cluster with low melt superheat[15]. At the same time the diffusion coefficient of Al is small, which restricts the diffusion rate of Al atom in the melt. When the alloy

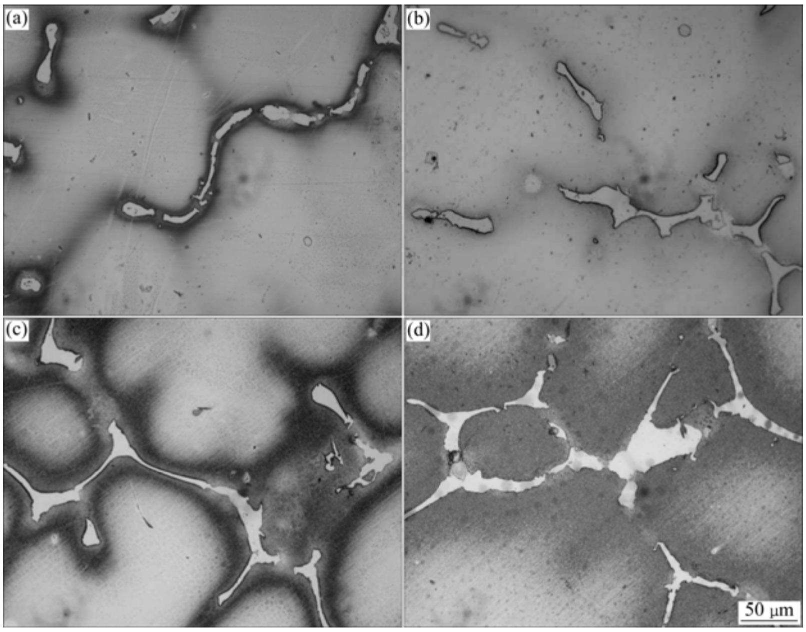

Fig.8 Morphologies of γ' phase in divorced eutectic of Al4Fe2Mn1.5 Monel alloy at different melt superheat: (a) 50 ℃; (b) 100 ℃; (c) 150 ℃; (d) 200 ℃

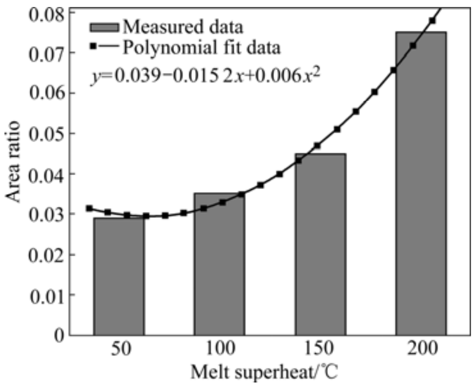

Fig.9 Area ratios of divorced eutectic γ' phase at different melt superheat

solidifies, the impelling velocity of solid/liquid interface is larger than the diffusion velocity of Al atom, and Al atom cluster can be trapped by solid/liquid interface. Thereby it restricts the diffusion of Al atom into interdendritic area. However, Al is the important element to form eutectic γ' phase. Subsequently, the volume fraction of eutectic γ' phase is less in the fully solidified structure at low melt superheat. However, with increasing melt superheat, the cluster will decrease and disappear. Meanwhile, the alloy becomes uniform. Al atom has larger diffusion coefficient and velocity in the liquid. During solidification, the diffusion velocity of Al atom is faster than the moving velocity of solid/liquid surface, and makes the Al atom migrate to the interdendritic area, leading to the increase of the fraction of eutectic γ' phase in the interdendritic area (as shown in Fig.8 and Fig.9).

~~**Fig.10** Morphologies of γ' phase in dendrite arm at different melt superheats: (a) 50 ℃; (b) 100 ℃; (c) 150 ℃; (d) 200 ℃~~

On the other hand, undercooling increases with increasing melt temperature[16], i.e., the irreversible atom cluster and the average size of atom group in the alloy become smaller, and even disappear with increasing temperature, thus decreasing the number of inhomogeneous nucleation sites and increasing the nucleation undercooling.

$$\Delta G^{*} \geqslant \frac{16\pi\sigma}{3(\Delta G_{\mathrm{V}}-\Delta G_{\mathrm{S}})} \quad (2)$$

~~W~~where ΔG_{V} is the ~~C~~change of volume free energy; ΔG_{S} is the ~~C~~change of area free energy; and σ is the ~~S~~ specific area free energy.

And XIAO[17] pointed out:

$$\Delta G_{\mathrm{V}} \propto \Delta T \quad (3)$$

~~W~~where ΔT is the undercooling.

From the relationship of these equations, the increase of undercooling leads to the increase of ΔG_{V} with increasing melt superheat. Furthermore, the critical nucleating energy will decrease if other parameters are not changed. Besides, the nucleating rate can be expresse~~s~~d as ~~the formula (4-4).~~

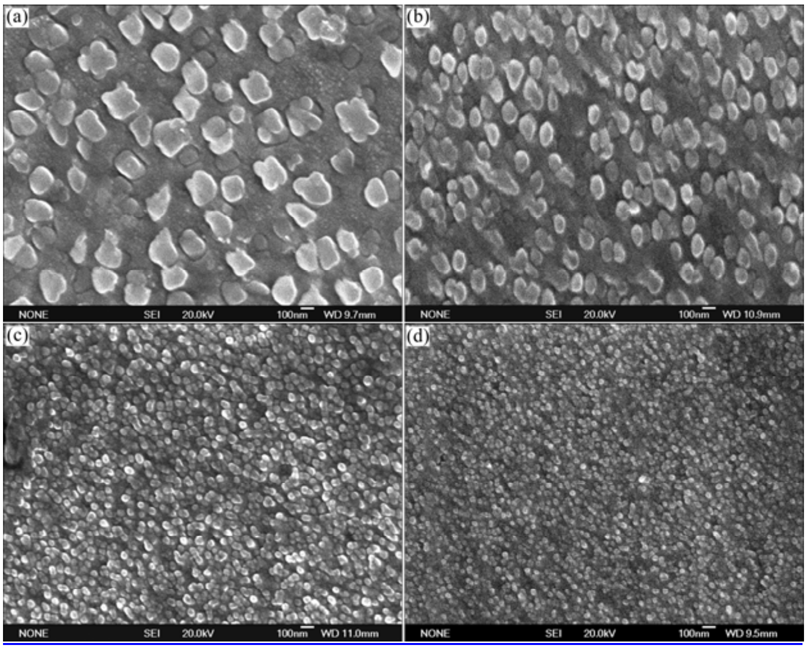

Fig.10 Morphologies of γ' phase in dendrite arm at different melt superheat: (a) 50 ℃; (b) 100 ℃; (c) 150 ℃; (d) 200 ℃

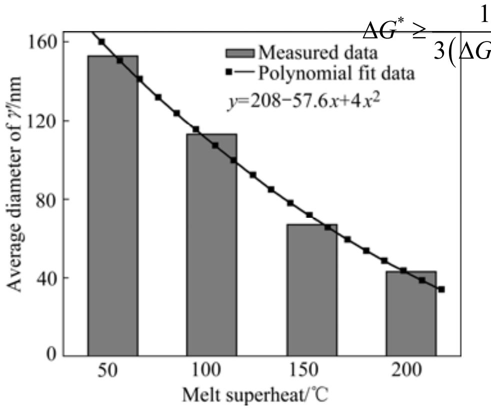

Fig.11 Diameters of γ' phase in dendritic arm at different melt superheat

$I=K\exp(-\Delta G^*/kT)\exp(-Q/kT)$

~~$$I=K\exp\left(-\Delta G^*/kT\right)\exp\left(-Q/kT\right)$$~~

(~~4-~~4)

~~W~~where I— is the nucleation rate;

K— is the proportional constant;

ΔG^* is the —nucleation energy;

Q— is the diffusion activation energy; k is the

—~~B~~Boltzmann constant; and

T— is the thermodynamics temperature.

According to Eq.~~formula~~ (~~4-~~4), the nucleation rate is sensitive to undercooling and it increases with the increase of undercooling~~-~~. At the same time, the critical nucleation radius can be expressed ~~as the formula (4-5):~~ as

$$r^*=\frac{2\sigma T_m}{L_m\Delta T}\tag{5}$$

~~**Fig.11** Diameters of γ′ phase in dendritic arm at different melt superheat~~

~~(4-5)~~

$$r^*=\frac{2\sigma T_m}{L_m\Delta T}$$

~~W~~where σ is the

—~~Sp~~specific surface energy; T_m is the

—melting point; L_m is the

—fusion heat; ΔT is the

—undercooling.

From ~~formula~~ Eq.(~~4-~~5), the critical nucleation radius —r^* decreases with increasing undercooling~~-~~, i.e.~~,~~ the atom cluster which ~~was~~ is less than critical nucleation radius can become stable nucleation site with increasing undercooling. Obviously, whatever the nucleation rate I increases or the critical nucleation radius decreases can refine grains under the large supercooling, thus leading to the refinement of grains. So γ dendrite becomes finer with the increase of melt superheat (as shown in Fig.6 and Fig.7).

For γ' phase distributed on the dendrite arm, the critical nucleating energy can also be expressed in the form of

$$\Delta G^*\geqslant\frac{16\pi\rho}{3(\Delta G_V-\Delta G_S)}\tag{6}$$

~~(4-6)~~

~~W~~where ΔG_V and ΔG_S represent the changes of chemical free enthalpy and strain energy per unit volume precipitation of γ' phase, respectively~~.——~~, and ρ is the interface free energy of $\gamma'\rightarrow\gamma$ per unit phase.

Meanwhile, from ~~literature~~ Ref.[17]:

$$\Delta G_V\propto\Delta X,\ \Delta G_V\propto\Delta\theta\tag{7}$$

~~W~~where ——ΔX is the supersaturation of solute in γ solid solution; and $\Delta\theta$~~.~~

— is the undercooling of solute in γ solid solution.

According to ~~e~~Equatio~~n~~ (~~4-~~6), —ΔG^* decreases with the decrease of —ρ and increase of ΔG_V~~——T~~, thus has high nucleation rate of γ' phase. γ' phase is the ~~diffuse~~ diffusing phase transformation product of γ solid solution. This process needs a certain incubation period. In this period, the lean solute area and rich solute area form in the supersaturation γ solid solution, which is beneficial to the precipitation of γ' phase from γ solid solution. The microstructure of the alloy becomes uniform and dendritic segregation decreases with increasing melt superheat. The diffusion distance of elements in solid phase transformation becomes large, which causes the difficulty to form two areas, and lowers the formation temperature of γ' phase and increases undercooling. It can be seen from ~~e~~Equatio~~n~~ (~~4-~~7) that, the increase of undercooling —$\Delta\theta$ leads to the increase of—— ΔG_V. Therefore, the nucleation rate of γ' precipitation phase increases with increasing the undercooling. In addition, the growth time of γ' phase reduces with the increase of melt superheat. So the size of γ' precipitation phase decreases when the melt superheat increases (as shown in Fig.10 and Fig.11).

As discussed above, Al4Fe2Mn1.5 Monel alloy has larger nucleation rate and less critical nucleation radius with the increase of melt superheat. Meanwhile, the primary dendrite arm of γ matrix is gradually melted off and SDAS gradually becomes smaller (as shown in Fig.6 and Fig.7). The eutectic γ' phase in the interdendritic area becomes larger (as shown in Fig.8 and Fig.9) and the average diameter of γ' phase distributed on the dendritic arm also becomes smaller (as shown in Fig.10 and Fig.11).

5 Conclusions

1) The microstructure of Al4Fe2Mn1.5 Monel alloy consists of dendritic γ matrix and γ' phase(Ni_3Al) which has two morphologies. One distributes dispersedly on the dendritic arm and in the transition area between dendritic arm and interdendritic area, which has separated particle form and petalform, respectively. The other is divorced eutectic γ' which distributes in the interdendritic area at different melt superheat.

2) With the increase of melt superheat, dendritic γ matrix becomes finer, and the primary dendritic arm is gradually melted off. At the same time, the secondary dendritic arm spacing decreases. The fraction of divorced eutectic γ' also becomes larger in the interdendritic area. The size of γ' on the dendritic arm gradually becomes smaller. When the melt superheat is 200 ℃, dendritic γ matrix is finer, the fraction of eutectic γ' is larger, and the diameter of γ' phase distributed on the dendritic arm is smaller compared with those at other melt superheats.

References

[1] MENG Jia-yan. American Monel alloy system [J]. Development and Application of Materials, 1992, 7(1): 44−49. (in Chinese)

[2] XIANG Pei-sen. Heavy nonferrous metal materials processing directory [M]. Beijing: Metallurgical ~~industry~~ Industry ~~press~~Press, 1979: 328. (in Chinese)

[3] YUAN Chao, YANG Hong-cai, LIU Shi-gui. Aging crack trend of Monel K500 alloy [J]. Journal of Northeastern University, 1994, 15(2): 180−183. (in Chinese)

[4] YUAN Chao, YANG Hong-cai, WANG Zhi-xing, GUO Jian-ting. Precipitation and aging hardness in a high strength and corrosion resistant Ni-Cu alloy [J]. Journal of Northeastern University (Nature Science), 1997, 18(1): 82−85. (in Chinese)

[5] ~~S.K.~~GHOSH S K, ~~G.K.~~DEY G K, ~~R.O.~~DUSANE R O, ~~A.K.~~GROVER A K. Improved pitting corrosion behaviour of electrodeposited nanocrystalline Ni-Cu alloys in 3.0wt.%NaCl solution [J]. Journal of ~~alloys~~ Alloys and ~~compounds~~Compounds, 2006, 426(1/2): 235−243.

[6] ZHANG Hong-bin, LI Li-shan. Engineering properties of Monel K500 Ni-based corrosion resistant alloy [J]. Special Steel Technology, 1996, (3): 31−35. (in Chinese)

[7] CAI Zhen-jiang. Application of Monel alloy in our country's ship [J]. Ship and Boat, 2003, (4): 20−21. (in Chinese)

[8] ~~O.S.~~ES-SAID O E, ~~K.~~ZAKHARIA K, ~~Z.~~ZAKHARIA Z, ~~C.~~VENTURA C, ~~D.~~PFOST D, ~~P.~~CRAWFORD P, ~~T.~~WARD T, ~~D.~~RAIZK D, ~~J.~~FOYOS J, ~~R.~~MARLOTH R. Failure analysis of Monel K500 (Ni-Cu-Al alloy) bolts [J]. Engineering Failure Analysis, 2000, 7: 323−332.

[9] LI De, XU Jiu-quan. Effects of aging on microstructure and hardness of Monel alloy [J]. Journal of Liaoning Institute of Technology, 1997, 17(2): 52−54. (in Chinese)

[10] WANG Zhi-xing, LIU Shi-gui, YUAN Chao, YANG Hong-cai. Strength and toughness of Ni-Cu based Monel K500 alloy [J]. The Chinese Journal of Nonferrous Metals, 1994, 4: 184−187. (in Chinese)

[11] ~~G.K.~~DEY G K, ~~R.~~TEWARI R, ~~P.~~RAO P, ~~S.L.~~WADEKAR S L, ~~P.~~MUKHOPADHYAY P. Precipitation hardening in nickel-copper base alloy Monel K 500 [J]. Metallurgical and Materials Transactions A, 1993, 24: 2709.

[12] YUAN Chao, LIU Shi-gui, YANG Hong-cai, WANG Zhi-Xing. Deposition behavior of precipitation in Monel K500 alloy [J]. Physics Examination and Testing, 1994, (6): 9−13. (in Chinese)

[13] ZHAO Dong-mei, DONG Qi-ming, LIU Ping, KANG Bu-xi, JIN Zhi-hao. Investigation of aging process of ultra-strength Cu-Ni-Si alloy [J]. Transactions of Materials Heat Treatment, 2002, 23(2): 20−23.

[14] SU Yan-qing, GUO Jing-jie, LIU Gui-zhong. Melt quality control of nonferrous alloy in vacuum melting [M]. Harbin: Harbin Institute of Technology Press, 2005: 31. (in Chinese)

[15] YIN Feng-shi, SUN Xiao-feng, HOU Gui-chen, ZHENG Qi, GUAN Heng-rong, HU Zhuang- lin. Effects of melt superheat treatment on segregation of M963 alloy [J]. Rare Metal Materials and Engineering, 2004, 33(6): 659−661. (in Chinese)

[16] WANG Zhen, LI Jin-guo, ZHAO Nai-ren, JIN Tao, ZHANG Jing-hua. Effects of melt temperature treatment on melt structure and solidification microstructure of nickel-based single crystal superalloy [J]. Acta Metallurgica Sinica, 2002, 38(9): 920−924. (in Chinese)

[17] XIAO Ji-mei. Alloy phase and phase transformation [M]. Beijing: Metallurgical Industry Press, 1987: 233. (in Chinese)

(Edited by YUAN Sai-qian)

带格式的: 项目符号和编号

带格式的: 项目符号和编号